

Article

Chromium–Aluminum Coatings for Oxidation Protection of Titanium–Aluminum Intermetallic Alloys

Almaz Nazarov ¹, Alexey Maslov ¹, Elena Korznikova ^{1,2,*}  and Kamil Ramazanov ¹

¹ Department of Mechanical Engineering Technology, Ufa University of Science and Technology, Ufa 450076, Russia; nazarov_almaz15@mail.ru (A.N.)

² Polytechnic Institute (Branch) in Mirny, North-Eastern Federal University, Mirny 678170, Russia

* Correspondence: elena.a.korznikova@gmail.com

Abstract: This article explores the utilization of cathodic-arc deposition Cr–Al overlay coatings as oxidation protection for Ti–Al–Nb intermetallic alloys. The primary objective is to investigate PVD Al–Cr coatings deposited via cathodic-arc deposition without subsequent vacuum annealing. The microstructure, phase, and chemical composition of the coatings were characterized using scanning electron microscopy, energy-dispersive X-ray spectroscopy, and X-ray diffraction analysis. Isothermal exposure of samples in a laboratory air furnace was conducted, revealing the efficacy of Cr–Al coatings in protecting the Ti49–11Al–40Nb–1.5Zr–0.75V–0.75Mo–0.2Si (mass%) intermetallic alloy VTI-4 against oxidation. The findings highlight that the as-deposited coatings possess a layered structure and contain Al–Cr intermetallics. Post-exposure to the furnace without prior vacuum annealing results in coatings exhibiting a porous microstructure, raising concerns regarding oxidation protection. This investigation of Cr–Al coatings on a VTI-4 alloy substrate yields valuable insights into their nanolaminate structure and challenges associated with aluminum droplet fractions. The proposed additional vacuum heat treatment at 650 °C for 500 h effectively homogenizes the coating, leading to predominant Cr₂Al and Ti–Al phases. Additionally, the formation of diffusion layers at the “coating–substrate” interface and the presence of oxide barriers contribute to the coatings’ heat resistance. Our research introduces possibilities for tailoring coating properties for specific high-temperature applications in aerospace, energy, or industrial contexts. Further refinement of the heat treatment process offers the potential for developing advanced coatings with enhanced performance characteristics.

Keywords: coating; PVD; intermetallic; oxidation; Ti–Al alloy; cathodic-arc deposition



Citation: Nazarov, A.; Maslov, A.; Korznikova, E.; Ramazanov, K. Chromium–Aluminum Coatings for Oxidation Protection of Titanium–Aluminum Intermetallic Alloys. *Quantum Beam Sci.* **2023**, *7*, 36. <https://doi.org/10.3390/qubs7040036>

Academic Editors: Klaus-Dieter Liss and Rozaliya Barabas

Received: 30 July 2023

Revised: 14 October 2023

Accepted: 16 November 2023

Published: 20 November 2023



Copyright: © 2023 by the authors. Licensee MDPI, Basel, Switzerland. This article is an open access article distributed under the terms and conditions of the Creative Commons Attribution (CC BY) license (<https://creativecommons.org/licenses/by/4.0/>).

1. Introduction

Since the 2000s, Ti–Al alloys have attracted the attention of scientists, the aerospace industry, and internal combustion engine manufacturers due to their excellent high-temperature mechanical properties, good oxidation resistance, and relatively low density [1]. Ti–Al alloys can outperform Ti-based alloys and even some Ni-based superalloys in terms of specific strength and density [2,3]. Today, this group of intermetallic alloys is used for the manufacture of low-pressure turbine blades for jet engines and turbocharger rotors, as they are capable of operating in aggressive environments, especially for γ -TiAl alloys. However, the limits of the operating temperatures of unprotected alloys lie within 750–850 °C; above these values, bare Ti–Al alloys begin to form unprotected unstable oxide films of the TiO₂ type [4,5]. This phenomenon necessitates the protection of Ti–Al alloys from oxidation to ensure their performance at 900 °C and above [6], as well as new alloys and methods for their production [7–10].

An active search for ways to solve this industrial problem began more than 30 years ago. At the moment, there are three main ways to protect Ti–Al alloys: the first one is the application of overlay coatings using various technologies such as cathodic-arc deposition

or magnetron sputtering, the second is diffusion coatings, and the third is the so-called halogen effect [11,12]. In an overlay coating, the elements are deposited directly onto the substrate using different technologies, such as thermal spraying, or CVD or PVD processes. Diffusion coating consists of elements that diffuse into the substrate at elevated temperatures whereby a diffusion layer (interdiffusion can also occur) with a graded composition is formed. In the process named the "halogen effect", the substrate surface is first enriched with halogen at low temperatures before high-temperature exposure. During subsequent high-temperature exposure, the surface of the intermetallic Ti-Al alloy forms a protective alumina film on the coating surface.

Currently, various types of coatings and their combinations are being studied, the purpose of which is to protect the alloys under consideration from oxidation, such as the oxide coatings demonstrated in [13–16], intermetallic coatings explored in [17–19], as well as other methods to isolate alloy surfaces from aggressive environments described in [14,20,21]. Among other options, there is coating based on an Al-Cr system [22] that can be used for Ti-Al alloy protection.

In [23], a coating based on Ti-Al-Cr-Y/Zr was deposited using magnetron sputtering to protect Ti-48-2-2 (Ti-48Al-2Cr-2Nb at. %) and TNM-B1 (Ti-43.5Al-4Nb-1Mo-0.1B at. %) alloys during 1000 h of cyclic testing in air at temperatures ranging between 850 °C and 950 °C. The authors found that the Zr-containing coating on the TNM-B1 alloy proved to be less effective than the Y-containing layer. This probably occurred due to lower crack resistance during thermal cycling conditions. During a high-temperature oxidation protection test, the coatings showed a trend of depletion in chromium and aluminum due to mutual diffusion, which led to a change in their microstructure. The authors noticed that since the Ti-48-2-2 alloy contained 2 at. % Cr, chromium depletion was reduced for coatings deposited on this substrate material. The protective layer of thermally grown alumina overlay was stabilized in two ways: through the formation of a $\text{Ti}(\text{Cr},\text{Al})_2$ Laves phase upon short-term exposure, and through the formation of an orthorhombic U-phase and a cubic Z-phase upon long-term exposure. In conclusion, the authors demonstrated that the Ti-Al-Cr-Y intermetallic coating deposited on the Ti-48-2-2 alloy had the best oxidative behavior under cyclic exposure conditions.

In [24], the authors suggested a novel method to achieve surface protection and grain boundary modification for Nd-Fe-B magnets by using an annealed Al-Cr PVD coating. Cr plays an important role in enhancing coating hardness and changing the diffusion process. Therefore, Cr was introduced into an Al coating via sputtering and deposition using Al-Cr targets on Nd-Fe-B magnets. A coating with $\text{Al}_{70}\text{Cr}_{30}$ composition had a significantly higher hardness of 784 ± 10 HV, while an as-deposited Al layer had only a 205 ± 4 HV hardness, the same trend was observed for the scratch-test results. Subsequent annealing at 550 °C was performed to ensure diffusion of the Al atoms into the grain boundaries of the magnets. The authors noticed good adhesion between the Al-Cr coating and Nd-Fe-B magnet. In terms of corrosion resistance, it was observed that the introduction of Cr to achieve $\text{Al}_{70}\text{Cr}_{30}$ coating composition can significantly enhance the corrosion protection of the annealed coating due to its densification effect on the coating by modifying the Al diffusion process. It was also shown that Al atoms diffused into the substrate during the annealing process through the grain boundaries. In conclusion, the authors concludes that Al-Cr coatings can be effective hard anti-corrosion coatings with coercivity enhancement that help optimize the performance/cost ratio of rare earth magnets.

In [25], an Al-Cr-based coating was obtained on the surface of a Ti_2NbAl alloy using rf magnetron sputtering and double glow treatment by alternately depositing a layer of chromium and a layer of aluminum. The oxidation-resistant coating with an outer Al layer and inner Cr layer demonstrated good adhesion to the substrate due to the diffusion of Cr into the substrate and the interdiffusion between Cr and Al with the formation of an Al-Cr alloyed layer, which has great hardness. An acoustic emission curve, which was recorded using a scratch tester, indicated good bonding strength between Al/Cr coating and substrate. The morphology after the scratch test showed that the scratch was smooth

without disbanding, and the depth and breadth of scratch were changed uniformly. The results of the oxidation study showed that such a coating provides this alloy with corrosion protection at a temperature of 900 °C. After the oxidation test, no cracks were observed on the sample with the Al/Cr coating. The mass gain of the Ti₂NbAl alloy with the Al/Cr coating was less than that of the sample without an Al/Cr coating. The authors described the protection mechanism of the coating. After the thermal exposure coating demonstrated changes in the microstructure, a dense Al₂O₃ layer was formed on the coating surface, and Cr₂O₃ was produced under Al₂O₃ through the outward diffusion of Cr to protect the substrate during the isothermal oxidation tests. The process of titanium diffusion from the alloy into the outer layers of the coating was suppressed by the formation of intermetallic compounds of the Cr-Ti and Al-Ti systems. The elements' inter-diffusion seemed to be the reason for the good bonding strength between coating and Ti₂NbAl alloy.

The purpose of this work is to investigate overlay Cr-Al PVD coatings for Ti-Al alloy oxidation protection. Coatings were prepared using cathodic-arc deposition (Arc-PVD) without subsequent vacuum heat treatment. Using as-deposited coatings might be more attractive due to lower process costs, so vacuum treatment is not used in this work.

2. Materials and Methods

This study aimed to explore the application of Cr-Al coatings prepared via the cathodic-arc deposition (Arc-PVD) technique. Customized NNV-6.6-I1 equipment was used for coating deposition without subsequent annealing in a vacuum. This PVD system is equipped with two arc evaporators (chrome and aluminum cathodes) with pulsed cathode spot distribution without plasma filters and one thermionic cathode gas plasma source using non-self-sustained arc discharge, which was used for sample heating and deposition assistance.

This well-established method allows for the precise deposition of coatings on samples made of the Ti₄₉-11Al-40Nb-1.Zr-0.75V-0.75Mo-0.2Si (mass%) VTI-4 Ti-Al alloy based on the orthorhombic Ti₂NbAl titanium intermetallic alloy, a part of the Ti-11Al-40Nb group of alloys. Substrates with dimensions of 10 mm × 15 mm were ground using 1000-grade grinding paper and polished using 1-micrometer diamond suspension; then, they were ultrasonically cleaned in isopropyl alcohol before deposition.

During the deposition process, the samples underwent a carefully controlled procedure lasting 4 h. The first stage of process incorporated surface cleaning using gas discharge at an 800 V bias voltage and a 30 A non-self-sustained arc discharge current. After surface preparation, Al-Cr coatings with different parameters were deposited using cathodic-arc plasma source assistance with a 10 A discharge current. To ensure coating uniformity, the samples were rotated both on the table at a rotation speed of 1 rpm and around their axes at a speed of 20 rpm. These parameters were meticulously chosen to achieve optimal coating characteristics. The process parameters are presented in Table 1.

Table 1. Cr-Al coating deposition parameters.

Parameter	Value
Aluminum evaporator arc current	50 to 65 A (stepped)
Chromium evaporator arc current	From 100 to 80 A (estimated)
Bias	50 V
Vacuum chamber pressure	0.36 Pa

A Bruker D2 Phaser X-ray diffractometer was used for comprehensive analysis of the crystallographic structure of the coatings. The instrument was equipped with a highly sensitive solid-state position-sensitive LYNXEYE detector, and the DIFFRAC.SUITE software package 2020 allowed for the qualitative, quantitative, and full-profile analysis of diffraction patterns. The OriginLab Origin program was used to evaluate the X-ray diffraction patterns.

The structure of the coatings was investigated using a state-of-the-art Carl Zeiss Ultraplus ultra-high-resolution auto-emission scanning electron microscope (Carl Zeiss, Neubeuern, Germany) in BSE mode. The EDS analysis resolution was $0.3\ \mu\text{m}$, and the accelerating voltage was 15 kV. Cross-sectional BSE images of thin slices were obtained in the secondary electron mode, which allowed for a detailed look at the internal features and morphology of the coating. The samples were ground and polished with a $1\ \mu\text{m}$ thick diamond slurry prior to microstructure examination.

The distribution of chemical elements throughout the coating thickness was meticulously assessed using the INCA Energy system, which seamlessly integrated with the aforementioned microscope, providing valuable insights into the chemical composition of the coatings.

To evaluate the performance of the coatings under extreme conditions, heat resistance tests were performed in an oxidizing environment (laboratory air). In a Nabertherm N15/65HA furnace, the coated samples were subjected to a rigorous 500 h holding time at $650\ ^\circ\text{C}$, which simulates the challenging conditions under which coatings can operate in real-world conditions.

At regular intervals of 200, 300, and 400 h, the coated samples underwent further examination through X-ray diffraction analysis and scanning electron microscopy. This allowed for a detailed observation of any structural changes, degradation, or failure mechanisms that may have occurred during the prolonged exposure to elevated temperatures.

3. Results and Discussion

3.1. Microstructure

Figures 1–3 presented show detailed cross-sectional BSE images of the as-deposited Cr-Al coating. After deposition, the coating had a pronounced layered structure characterized by the presence of individual layers with a thickness of about $100\ \text{nm}$ (Figure 1). This layer thickness was due to the chosen deposition mode, namely, the table rotation speed during coating deposition. However, despite the aesthetic appeal of such a layered structure, it raises concerns in terms of thermal and mechanical resistance, as it may not provide optimal protection for the bulk of the material [26–30].

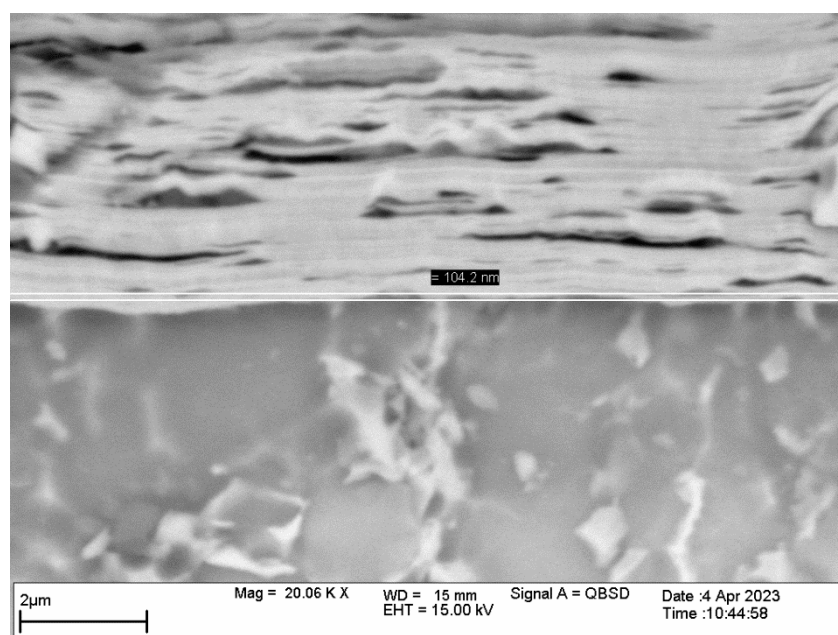


Figure 1. BSE image of layered structure of as-deposited Cr-Al coating on Ti-11Al-40Nb alloy.

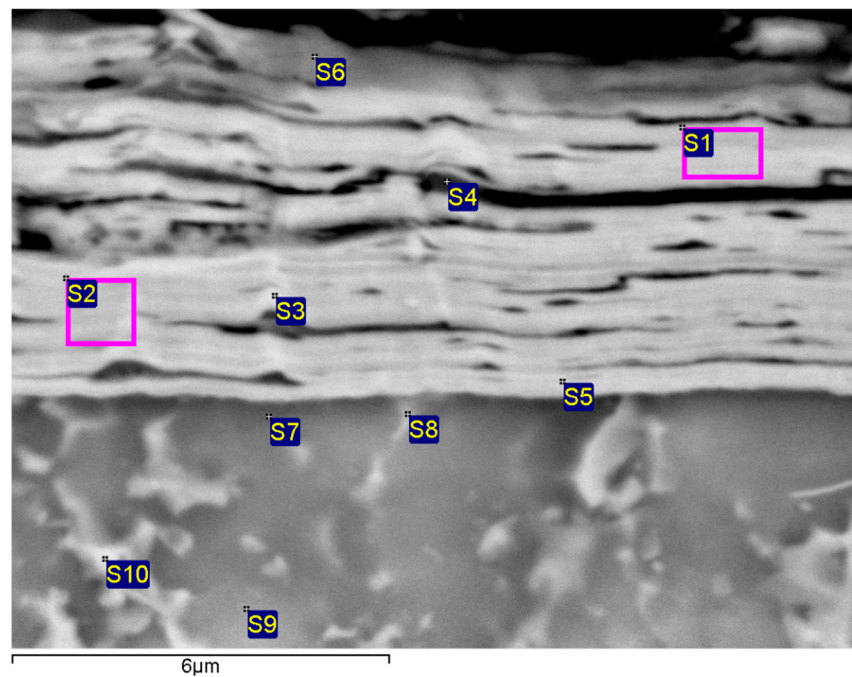


Figure 2. Chemical analysis of coating after deposition on Ti-11Al-40Nb alloy.

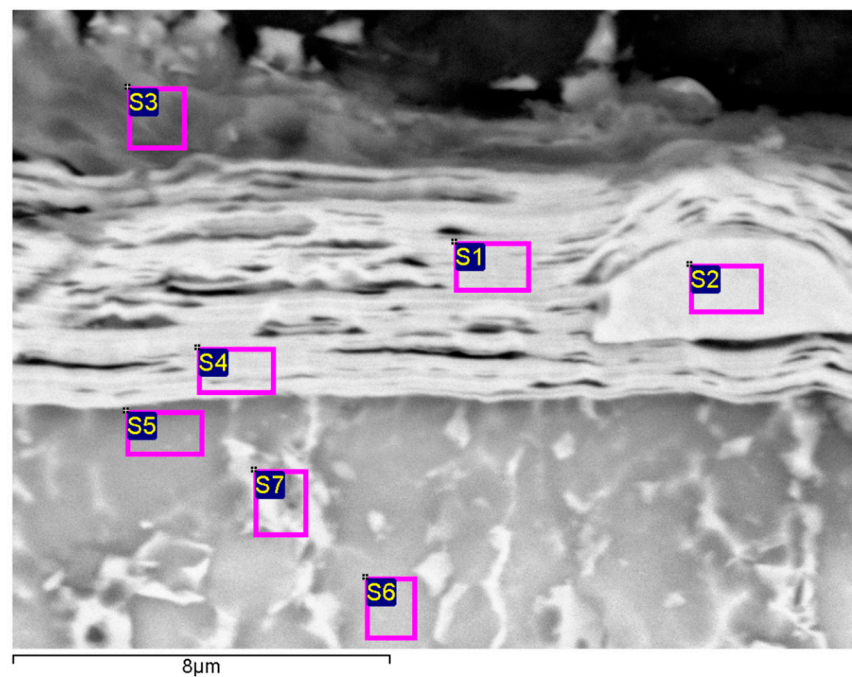


Figure 3. BSE image of Cr droplet in Cr-Al coating and the sites of EDS analysis.

To address this limitation, additional vacuum heat treatment is deemed necessary to enhance diffusion processes within the coating [30–34]. This strategic heat treatment promotes the intermixing of aluminum (Al) and chromium (Cr) atoms at the interfaces of the layered coating. As a result, diffusion-driven phenomena occur, leading to the formation of intermetallic phases within the coating.

The formation of intermetallic phases is of paramount importance as it introduces new microstructural features, significantly influencing the mechanical, thermal, and functional properties of the Al-Cr layered coatings. Consequently, understanding the role of diffusion in the behavior and performance of these coatings is crucial for optimizing their applications.

Moreover, heat treatment offers the opportunity to create structures within the coating with a tailorable set of properties [35–39]. By precisely controlling the heat treatment parameters, it becomes possible to form the desired properties of the coating, making it suitable for specific applications and environments.

In conclusion, the cross-sectional BSE images of the layered structure of the as-deposited Cr-Al coating reveal the presence of a distinct layered structure (see Figure 1). Therefore, additional vacuum heat treatment is necessary to enhance the diffusion processes and facilitate the formation of intermetallic phases. This diffusion-driven intermixing of Al and Cr atoms significantly impacts the microstructure and properties of the coating. Understanding these diffusion-based mechanisms is crucial in optimizing the behavior and performance of Al-Cr layered coatings, making them more suitable for oxidation protection applications in the realm of materials science and engineering.

The chemical composition analysis of the Cr-Al coating is summarized in Table 2. Despite the given gradients in the deposition mode, the aluminum content across the coating's cross-section remains relatively constant. Similarly, the chromium content remains stable, except for the "coating–substrate" interface zone, where chromium diffuses into the alloy, as observed in zones S7 and S8.

Table 2. EMF analysis results, wt. %.

Range	Al	Ti	Cr	Nb
S1	20.44	1.21	78.35	
S2	18.03	1.98	79.99	
S3	18.40	2.00	79.60	
S4	37.54	1.25	61.21	
S5	13.38	13.11	73.51	
S6	25.83		74.17	
S7	13.41	46.75		39.84
S8	6.24	39.89		53.87
S9	11.18	46.90		41.92
S10	7.24	33.47		59.29

Despite the gradients in metal content during the deposition process, the coating layers exhibit a remarkable difference in their chemical composition. Detailed energy-dispersive X-ray spectroscopy (EDS) analysis reveals that the coating consists of distinct alternating layers of intermetallic compounds, namely, Cr-Al, Cr_5Al_8 with 54.6% Cr and 45.4% Al, and Cr_2Al with 80% Cr and 20% Al. These findings are consistent with the results obtained from the X-ray diffraction (XRD) analysis.

In Figure 2, the dark layers correspond to the intermetallic compound Cr_5Al_8 , as observed in zone S4. Conversely, the light layers are attributed to intermetallic Cr_2Al , identified in zones S1, S2, S3, and S6. Interestingly, the deposition process conditions lead to alternating cycles of aluminum enrichment and depletion within the deposited layers.

These observations suggest that during the coating deposition, specific conditions are established, allowing the individual layers to undergo successive cycles of aluminum enrichment and depletion. Such unique conditions contribute to the formation of alternating intermetallic compound layers with distinct chemical compositions. This phenomenon plays a pivotal role in determining the overall properties and performance of the Cr-Al coating.

The understanding of the chemical composition and layering in the coating provides crucial insights into the structure–property relationships and guides the optimization of the coating's microstructure for tailored applications in various fields of materials science and engineering.

Figure 3 shows a macroscopic inclusion of a drop fraction from a chromium cathode (zone S2). It was probably the inclusions of these macro-particles that caused the loose and

discontinuous structure of the coating after exposure in the furnace for 500 h. The EDS analysis results are presented in Table 3.

Table 3. EDS analysis results, wt. %.

Spectrum	Al	Ti	Cr	Nb
S1	18.75	1.17	80.08	
S2		1.68	98.32	
S3	96.18		3.82	
S4	15.81	4.18	80.01	
S5	16.00	44.26		39.74
S6	11.96	46.80		41.24
S7	9.50	38.33		52.17

The results of BSE analysis reveal intriguing observations about the Cr-Al coating. Initially, after deposition, the coating exhibited a distinct layered structure. However, upon heating, the coating crystallized and underwent oxidation, leading to the development of numerous pores and discontinuities within its structure. Surprisingly, despite these imperfections, the coating demonstrated remarkable adhesion to the substrate and remained intact without peeling off or collapsing during the heating process.

Figure 4 depicts the coating's evolution during heating, illustrating the disappearance of its layered structure. This phenomenon suggests that as a result of the heating process, homogenization of the intermetallic phases within the coating occurred. This homogenization is further supported by the reduction in the degree of inhomogeneity in the distribution of aluminum and chromium across the coating's cross-section.

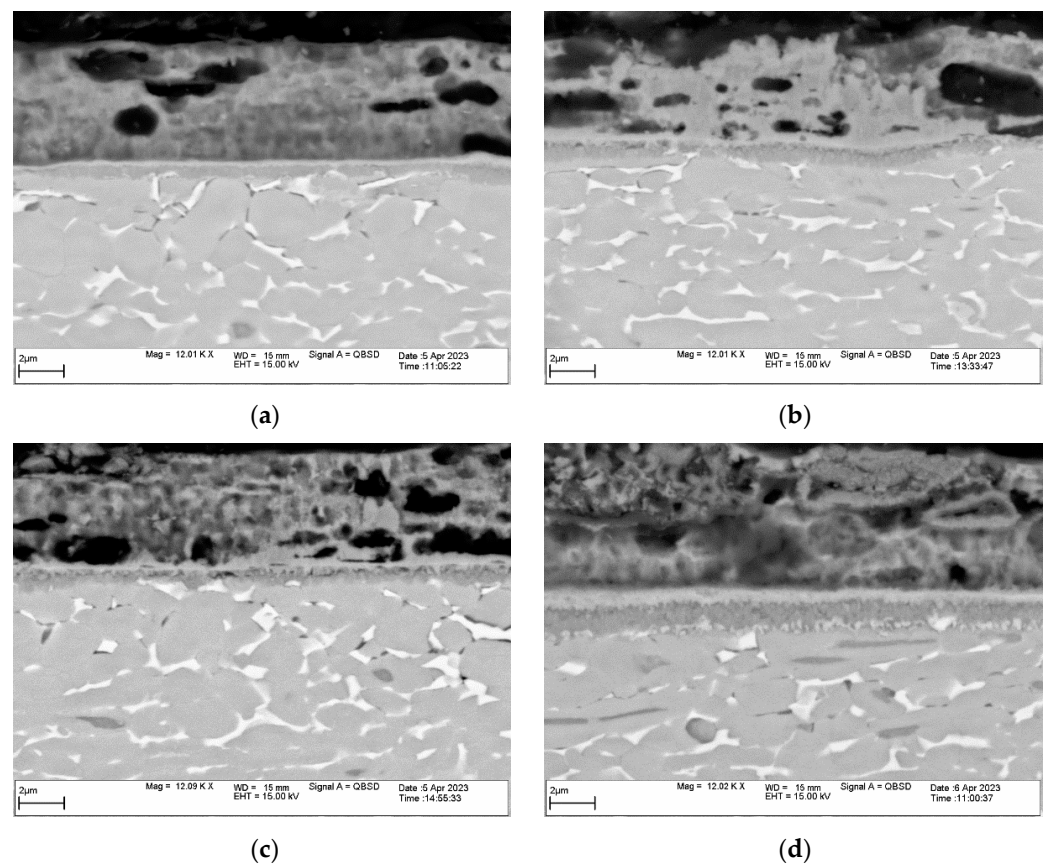


Figure 4. Cr-Al coating on Ti-11Al-40Nb alloy after 200 (a), 300 (b), 400 (c), and 500 (d) hours of exposure in furnace.

Interestingly, similar homogenization processes were reported in previous research involving bulk materials based on Ti-Al intermetallic phases. However, in this current study, the annealing was performed at a lower temperature but for an extended period (ranging from 200 to 500 h). This extended annealing duration allowed sufficient time for the intermetallic phases within the coating to reach a more uniform composition and distribution.

The nanolaminate structure of the coating's layers also played a significant role in facilitating the homogenization process. The unique nanolaminate arrangement of the layers enhanced the diffusion rate of aluminum and chromium atoms, promoting their intermixing and homogenization.

After 200 h of exposure to the annealing process, a distinct double diffusion zone became evident in the coating. This zone further expanded in thickness after 500 h of exposure (Figure 5). As the annealing process progressed, the coating's structure underwent gradual degradation, yet no macroscopic damage or failure was observed.

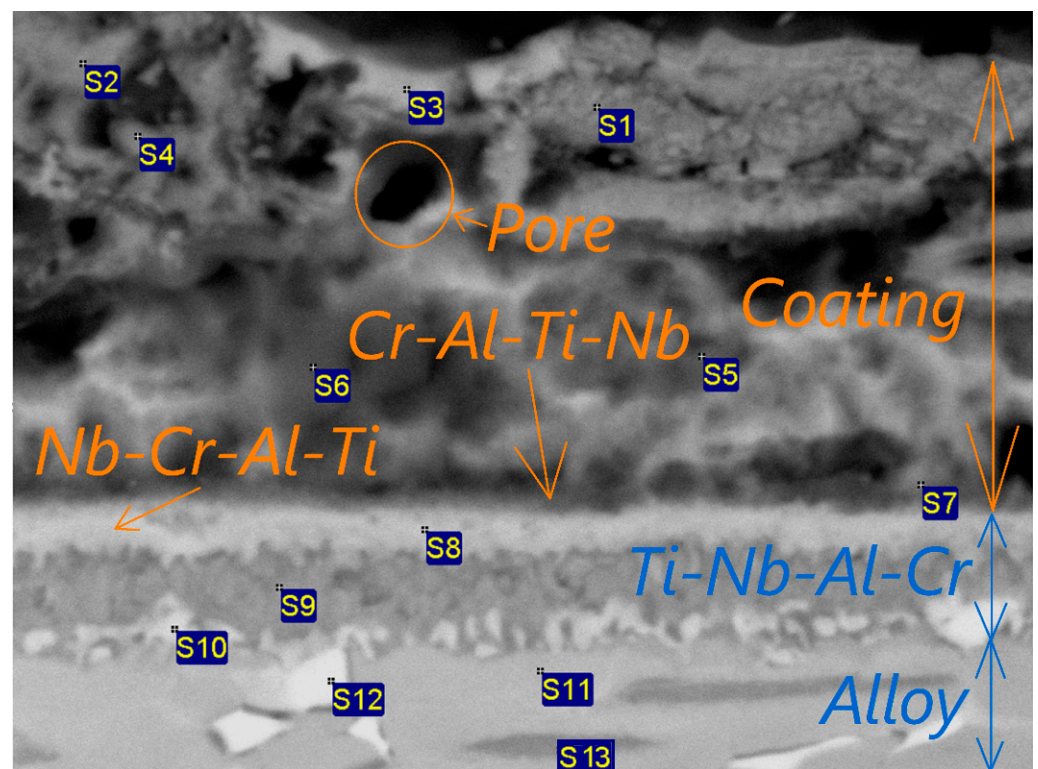


Figure 5. BSE image of Al-Cr coating on Ti-11Al-40Nb alloy after oxidation at 650 °C for 500 h and the sites of EDS analysis.

The ability of the coating to maintain its integrity despite undergoing crystallization, oxidation, and the presence of pores and discontinuities highlights its robustness and adhesion to the substrate. The homogenization of intermetallic phases and the formation of the double diffusion zone further add to the complexity of the coating's microstructure, influencing its mechanical and thermal properties.

In conclusion, the results of the BSE analysis presented in Figure 5 provide valuable insights into the behavior of the Cr-Al coating during heating. The observed disappearance of the layered structure, homogenization of intermetallic phases, and formation of the double diffusion zone are crucial in understanding the coating's response to thermal exposure. The coating's ability to withstand these changes without macroscopic damage underscores its potential for various applications in the realm of materials science and engineering. Further research on the coating's mechanical and thermal performance is essential to fully exploit its unique properties for practical applications.

After 500 h of testing, the Cr-Al coating structure exhibited significant porosity, although no macroscopic failures were evident. The analysis revealed the formation of two diffusion layers (spectra S8 and S9), along with the precipitation of Nb-Ti-Al (S10). Surprisingly, the distribution of chemical elements indicated the presence of oxygen throughout the coating cross-section due to non-uniformities and pores, contradicting previous findings [24]. However, no diffusion of oxygen into the alloy was detected, likely attributed to the presence of dense diffusion layers of Nb-Cr-Al-Ti (spectrum S8) and Ti-Nb-Al-Cr (spectrum S9). These layers acted as barriers, hindering oxygen diffusion, while containing titanium that diffused from the alloy. The distribution of the elements is presented in Table 4. Despite the observed porosity, the coating displayed promising resilience, with no detectable macroscopic failures, showcasing its potential for various applications in demanding environments. Further investigation into the coating's microstructure and properties is essential to fully comprehend its behavior under prolonged testing conditions.

Table 4. EDS analysis results of Al-Cr coating after oxidation at 650 °C for 500 h.

Range	O	Al	Ti	Cr	Nb
S1		24.55		65.05	
S2	15.36	20.83		53.07	
S3	8.95	14.96		61.54	
S4	22.34	21.30		45.38	
S5		7.00	7.41	60.60	
S6	11.59	14.63	7.37	53.99	
S7	6.28	19.12	12.89	52.88	8.85
S8		23.27	21.27	23.71	31.76
S9		28.75	37.72	1.94	31.60
S10		20.68	36.46		42.86
S11		13.39	46.59		40.02
S12		9.44	39.12		51.44
S13		11.34	49.96		38.70

All results in weight%.

In general, our results correlate with those in Ref. [35], where a thermal treatment mode was selected to achieve optimal properties of the Elinvar alloy. It was demonstrated that the alloy's structure was improved through the application of thermal stresses, as well as the formation and dissolution of intermetallic compounds during the thermal treatment process.

3.2. X-ray Diffraction Analysis

Figures 6–8 show the results of the X-ray phase analysis of the coatings after deposition and during isothermal annealing. The shooting was carried out after 200, 300, 400, and 500 h. The scattering vector ($1/\text{Å}$) on the X-axis was calculated using the formula $Q = 4 \times \pi / 1.54 \times \sin\left(\frac{2\theta/2}{180 \times \pi}\right)$.

The diffraction pattern obtained from the as-deposited Cr-Al coating exhibits distinct reflections corresponding to the intermetallic phases present within the coating, characteristic of the Al-Cr system. Additionally, titanium reflections associated with the substrate material are also evident in the diffraction pattern due to the diffractometer operation mode. This suggests that the coating is composed of a combination of intermetallic phases from the Al-Cr system and the substrate material, which is primarily composed of titanium-containing phase Ti_2AlNb .

Peak broadening in the diffraction pattern indicates that the coating has not undergone complete crystallization. This suggests that the crystalline structure of the coating is not fully formed, possibly due to the presence of defects (such as molten macro-parts), disordered regions, or incomplete atomic rearrangement during the coating process, because sample heating using a gas-plasma source was not enough to reach crystallization temperature.

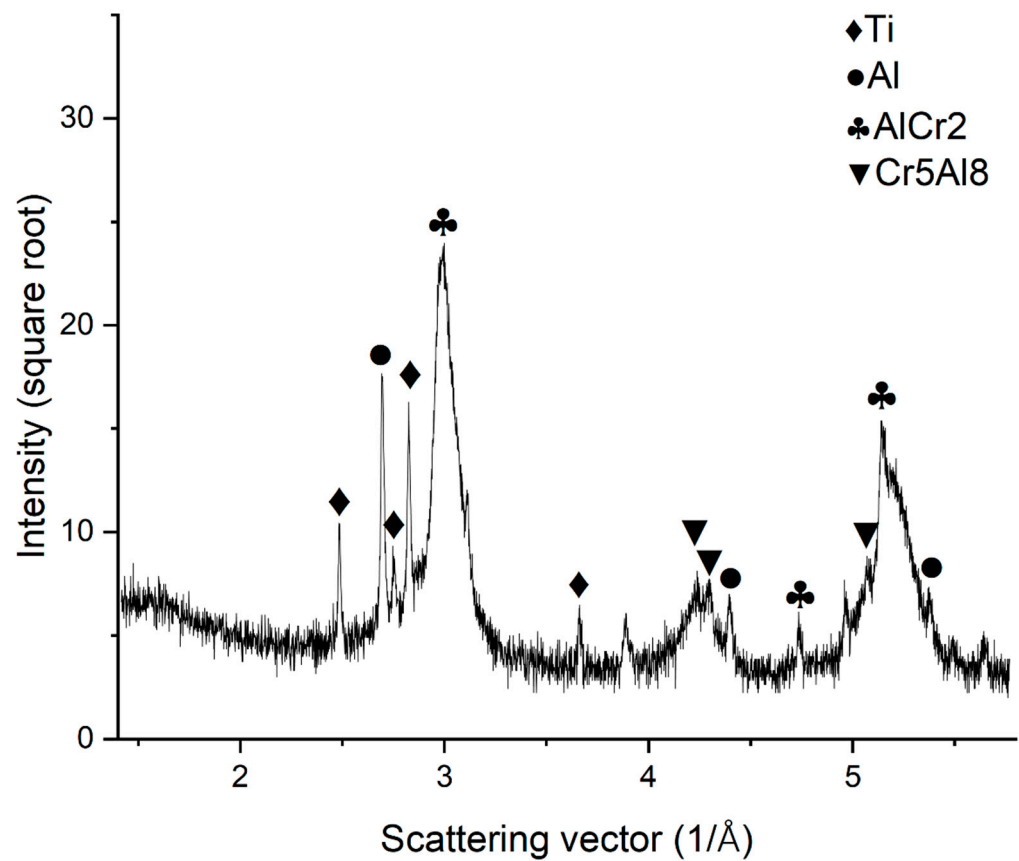


Figure 6. XRD diffraction pattern of as-deposited Cr-Al on Ti-11Al-40Nb alloy, square root of intensity.

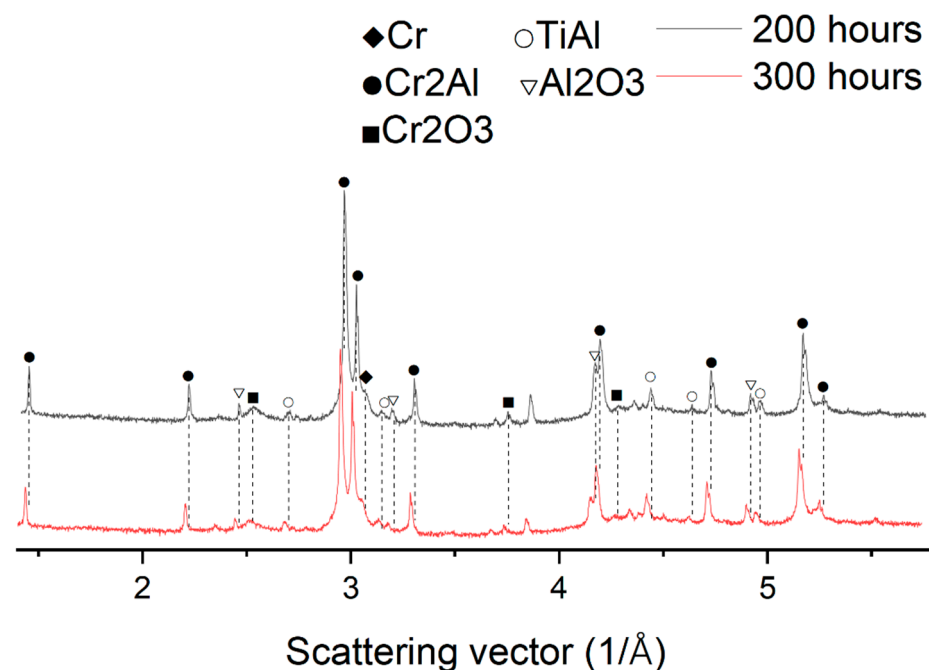


Figure 7. XRD patterns of Cr-Al coating on Ti-11Al-40Nb alloy after 200 and 300 h of exposure in furnace, square root of intensity.

Furthermore, the diffraction pattern shows multiple X-ray reflections in the coating, which can be attributed to its nanolayer structure, as observed in the electron microscopy results. The nanolayer structure of the coating results in multiple interfaces between the layers, leading to additional diffraction peaks. These peaks are a consequence of the

periodic arrangement of the nanolayers and the diffraction of X-rays from each interface. It is worth noting that the coating's thickness, composition, and micro stresses also might be reasons for such a peak pattern.

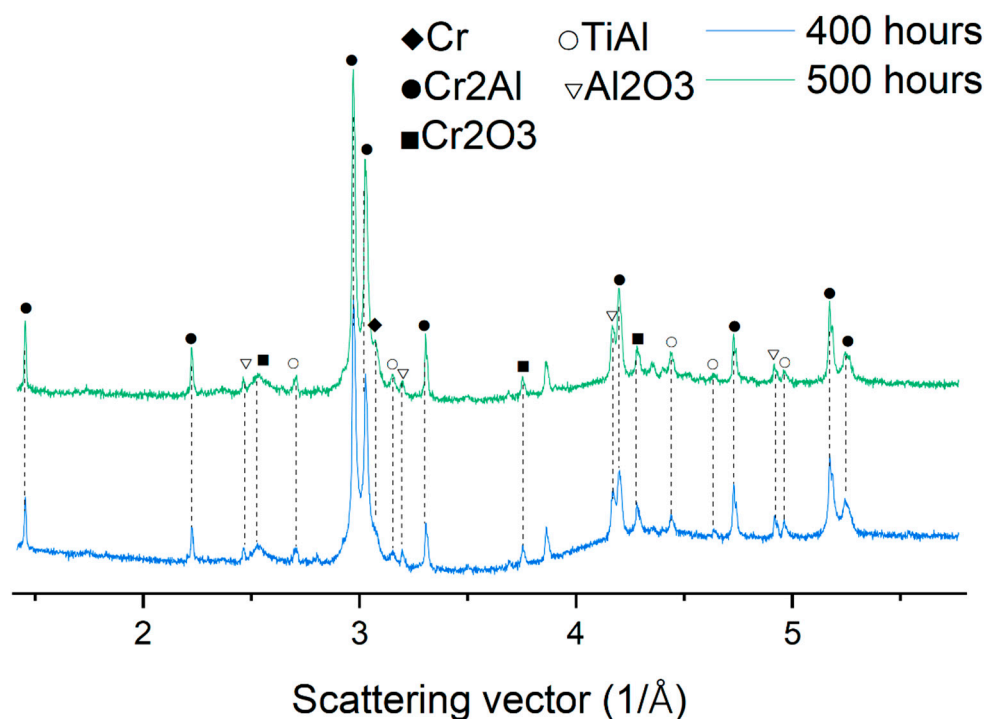


Figure 8. XRD patterns of Cr-Al coating on Ti-11Al-40Nb alloy after 400 and 500 h of exposure in furnace, square root of intensity.

The combination of incomplete crystallization and the nanolayer structure in the coating introduces complexities in the diffraction pattern, making the analysis more intricate. Nonetheless, these characteristics provide valuable insights into the microstructural features of the Cr-Al coating, and they are crucial in understanding its properties and performance in various applications.

This study of coating behavior reveals interesting insights into the process of deposition and crystallization. Initially, after deposition, the coatings do not fully crystallize, but upon holding in the furnace, they undergo further transformation, leading to the formation of an Cr_2Al intermetallic compound (See Figures 7 and 8). This suggests that heat treatment plays a crucial role in achieving the desired crystalline structure and properties of the coatings.

One of the key aspects studied is the heat resistance of the coated samples. It was found that during the heat resistance testing, a mixture of Cr_2O_3 - Al_2O_3 oxides forms within the coating. Surprisingly, this mixture exhibits excellent adhesion to the substrate and does not exfoliate, which are crucial properties for any effective coating. However, the coating shows a porous and uneven structure, which may be an area for further improvement.

The results obtained from the qualitative X-ray phase analysis align with those of the chemical energy-dispersive analysis, confirming the presence of chromium oxides as the predominant component of the coating. This finding is consistent with the chosen mode of coating deposition, where intentional emphasis was placed on the predominance of chromium.

Furthermore, the back-scattered electron microscopy (BSE) results corroborate the energy-dispersive X-ray spectroscopy (EDS) findings, reinforcing the accuracy and reliability of the experimental data. The combination of XRD, EDS, and BSE techniques provides a comprehensive understanding of the coating's composition and structure.

Interestingly, this study also reveals that during annealing, not only do chromium and aluminum interact with each other to form Cr_2Al , but aluminum also partially reacts with titanium, leading to the formation of a titanium–aluminum intermetallic compound TiAl . This observation highlights the complex chemical processes that take place during heat treatment and emphasizes the need for precise control over the parameters to achieve the desired coating properties.

The porous and uneven structure of the coating resulting from the interaction of chromium, aluminum, and oxygen may offer unique opportunities for specific applications. For instance, the porosity might enhance certain mechanical or catalytic properties, making the coating suitable for specific purposes where a high surface area is desirable.

The findings from this study pave the way for further research and optimization of the coating process. By understanding the mechanisms behind crystallization, phase formation, and interactions between different elements, researchers can fine-tune the deposition and heat treatment processes to tailor the coatings for specific applications.

4. Conclusions

The study of Cr–Al coatings deposited on a substrate made of a VTI-4 alloy of the Ti-11Al-40Nb system revealed a unique nanolaminate structure consisting of intermetallic compounds with two stoichiometries— Cr_2Al and Cr_5Al_8 . This layered structure poses both opportunities and challenges for coating applications, requiring further research and heat treatment.

To address the challenges posed by the presence of droplet aluminum fractions in the coating, additional vacuum heat treatment is proposed. The goal of this heat treatment is twofold: first, to reduce the destructive effects of the aluminum droplets, and second, to achieve a continuous and more homogenized structure in the coating.

The researchers have established that annealing the coating at a temperature of $650\text{ }^\circ\text{C}$ for a duration of 500 h leads to the homogenization of intermetallic compounds. As a result, the predominant phases that form after annealing are Cr_2Al and TiAl . This indicates that the heat treatment is effective in transforming the coating into a more desirable composition, with a reduced presence of the less desirable Cr_5Al_8 phase.

In addition, heat treatment under these conditions promotes the formation of two diffusion layers at the interface between the coating and the substrate. These diffusion layers contain different ratios of Nb, Cr, Ti, and Al, indicating the formation of complex chemical interactions at the interface. This is an important result because it indicates that heat treatment affects not only the coating itself, but also the composition and structure at the coating–substrate interface.

Furthermore, the formation of these diffusion layers, as well as the presence of Cr_2O_3 and Al_2O_3 oxides, is a barrier that prevents oxygen from penetrating into the substrate. This is a very important aspect indicating the high heat resistance of the developed coatings. resistance to oxygen penetration is very important as it ensures that the properties and integrity of the substrate are maintained, even at high temperatures.

In conclusion, this study of Cr–Al coatings on a VTI-4 alloy substrate provides valuable insights into their nanolaminate structure and the challenges associated with droplet aluminum fractions. The proposed additional vacuum heat treatment at $650\text{ }^\circ\text{C}$ for 500 h successfully homogenizes the coating, forming predominant phases of Cr_2Al and TiAl . The formation of diffusion layers at the “coating–substrate” interface and the presence of oxide barriers further contribute to the heat resistance of the coatings. This research opens up opportunities for tailoring coatings’ properties for specific applications in high-temperature environments, such as in aerospace, energy, or industrial settings. Further optimization and fine-tuning of the heat treatment process can lead to the development of even more advanced coatings with enhanced performance characteristics.

Author Contributions: Conceptualization, A.N. and A.M.; methodology, A.N.; investigation, A.M.; writing—rough preparation, A.M.; writing—reviewing and editing, E.K.; project administration, K.R. All authors have read and agreed to the published version of the manuscript.

Funding: The study was supported by the Russian Science Foundation, grant number 22-29-01463.

Institutional Review Board Statement: Not Applicable.

Informed Consent Statement: Not applicable.

Data Availability Statement: Data are available from the corresponding author upon reasonable request.

Acknowledgments: The authors are grateful to I. Ramazanov, R. Nafikov, and K. Vostretsova for assisting with the XRD and BSE analyses, as well as to A. Pozdnyakov and A. Likhter for their help in preparing the materials.

Conflicts of Interest: The authors declare no conflict of interest.

References

1. Lim, H.P.; Liu, W.Y.H.; Melvin, G.J.H.; Jiang, Z.T. A brief review of the phase structure, oxidation kinetics and mechanical properties of complex Ti-Al alloys. *Materials* **2021**, *14*, 1677. [[CrossRef](#)] [[PubMed](#)]
2. Li, Y.; Dai, J.; Song, Y. Progress in research on the basic principles of studying the oxidation behavior of Ti-Al alloys and the effect of alloying. *Metals* **2021**, *11*, 985. [[CrossRef](#)]
3. Appel, F.; Paul, J.D.H.; Ehring, M. *Gamma Aluminide Titanium Alloys: Science and Technology*; John Wiley & Sons: New York, NY, USA, 2011.
4. Brady, M.P.; Brindley, V.J.; Smyalek, J.L.; Locci, I.E. Oxidation and protection of titanium gamma aluminides. *JOM* **1996**, *48*, 46–50. [[CrossRef](#)]
5. Zhao, L.; Zhang, Y.; Zhu, Y.; Lin, J.; Ren, Z. Oxidative behavior of γ -TiAl alloys at 900 °C in air. *Mater. High Temp.* **2016**, *33*, 234–240. [[CrossRef](#)]
6. Swadźba, R.; Laska, N.; Bauer, P.P.; Krztoń, H. Effect of pre-oxidation on cyclic oxidation stability of γ -TiAl at 900 °C. *Corros. Sci.* **2020**, *177*, 108985. [[CrossRef](#)]
7. Kenel, K.; Lis, A.; Dawson, K.; Stiefel, M.; Pechnik, K.; Barras, J.; Wegener, K. Mechanical performance and oxidation resistance of an ODS γ -TiAl alloy processed by spark plasma sintering and laser additive manufacturing. *Intermet* **2017**, *91*, 169–180. [[CrossRef](#)]
8. Kenel, K.; Dawson, K.; Barras, J.; Houser, K.; Dasargiri, G.; Bauer, T.; Wegener, K. Microstructure and stability of oxide particles in a novel γ -TiAl ODS alloy treated by spark plasma sintering and laser additive manufacturing. *Intermet* **2017**, *90*, 63–73. [[CrossRef](#)]
9. Prokopets, A.D.; Bazhin, P.M.; Konstantinov, A.S.; Chizhikov, A.P.; Antipov, M.S.; Avdeeva, V.V. Structural Features of TiB₂/TiAl/Ti₆Al₄V Layered Composite Material Obtained by Unlimited SHS Compression. *Lett. Mater.* **2021**, *300*, 130165. [[CrossRef](#)]
10. Bazhina, A.; Chizhikov, A.; Konstantinov, A.; Khomenko, N.; Bazhin, P.; Avdeeva, V.; Chernogorova, O.; Drozdova, E. Structure, phase composition and mechanical characteristics of layered composite materials based on TiB/xTi-Al/ α -Ti (x = 1, 1.5, 3) obtained by combustion and high-temperature shear deformation. *Mater. Sci. Eng. A* **2022**, *858*, 144161. [[CrossRef](#)]
11. Pflumm, R.; Friedle, S.; Schütze, M. Oxidation Protection of γ -TiAl Based Alloys—Review. *Intermetallides* **2015**, *56*, 1–14. [[CrossRef](#)]
12. Schütze, M. The Role of Surface Protection for the High Temperature Performance of TiAl Alloys. *JOM* **2017**, *69*, 2602–2609. [[CrossRef](#)]
13. Wang, J.; Kong, L.; Li, T.; Xiong, T. New TiAl₃/Al₂O₃ composite coating on γ -TiAl alloy and evaluation of oxidation performance. *Appl. Surf. Sci.* **2016**, *361*, 90–94. [[CrossRef](#)]
14. Simova, V.; Knittel, S.; Cavarroque, M.; Martinou, L.; Klemberg-Sapega, J.E. Amorphous Si-B-C-N coatings for protection against high-temperature oxidation of the γ -TiAl alloy. *Surf. Coat. Technol.* **2022**, *442*, 128544. [[CrossRef](#)]
15. Lin, H.; Liang, W.; Miao, Q.; Li, S.; Ding, Z.; Cui, S.; Yu, H. Creation of a self-supplied Al₂O₃-Y₂O₃ coating for γ -TiAl alloy with enhanced oxidation protection. *Appl. Surf. Sci.* **2020**, *522*, 146439. [[CrossRef](#)]
16. Wang, J.; Kong, L.; Li, T.; Xiong, T. Oxidation performance of TiAl₃ bonded thermal barrier coatings on γ -TiAl alloy. *J. Therm. Spray Technol.* **2015**, *24*, 467–475. [[CrossRef](#)]
17. Wang, Q.; Wu, W.-Y.; Jiang, M.-Y.; Cao, F.; Wu, H.-X.; Sun, D.-B.; Yu, H.-Y.; Wu, L.-K. Improved TiAl Alloy Oxidation Performance with New Al-Si Composite Coating. *Technol. Surf. Coat.* **2020**, *381*, 125126. [[CrossRef](#)]
18. Bauer, P.P.; Laska, N.; Swadźba, R. Improving the oxidation resistance of γ -TiAl by magnetron sputtering based on aluminum and silicon. *Intermetallides* **2021**, *133*, 107177. [[CrossRef](#)]
19. Xu, Y.; Shi, P.; Qiu, J.; Wu, A.; Cui, S.; Li, Z.; Tao, X. Oxidation and self-healing characteristics of MoSiAlY coating on γ -TiAl substrate by surface fusion method. *Vacuum* **2019**, *165*, 148–156. [[CrossRef](#)]
20. Fröhlich, M.; Braun, R.; Leyens, S. Oxidation resistant coatings combined with thermal barrier coatings on γ -TiAl alloys for high temperature applications. *Surf. Coat. Technol.* **2006**, *201*, 3911–3917. [[CrossRef](#)]
21. Bazhina, A.D.; Bazhin, P.M.; Chizhikov, A.P.; Konstantinov, A.S.; Stolin, A.M. Influence of high-temperature annealing on the structure of titanium aluminide materials obtained by combustion and high-temperature shear deformation. *Intermetallics* **2021**, *5*, 107313. [[CrossRef](#)]
22. Chen, Z.; Geng, L.; Qu, W.; Wang, J.; Chen, M.; Li, C.; Wang, F. Characteristics and hot corrosion resistance of co-deposition layers with different activators and Al-Cr ratios. *Corros. Sci.* **2022**, *202*, 110320. [[CrossRef](#)]

23. Laska, N.; Brown, R.; Knittel, S. Oxidation performance of Ti-Al-Cr-based protective coatings deposited on γ -TiAl Ti-48-2-2 and TNM-B1 alloys. *Technol. Surf. Coat.* **2018**, *349*, 347–356. [[CrossRef](#)]
24. He, J.; Liao, X.; Lan, X.; Qiu, W.; Yu, H.; Zhang, J.; Liu, Z. Annealed Al-Cr Coating: A hard anti-corrosion coating with grain boundary modification effect for Nd-Fe-B magnets. *J. Alloys Compd.* **2021**, *870*, 159229. [[CrossRef](#)]
25. Yang, Z.; Liang, W.; Miao, K.; Chen, B.; Ding, Z.; Roy, N. Oxidative behavior of Al/Cr coating on Ti₂AlNb alloy at 900 °C. *Mater. Res. Express* **2018**, *5*, 046408. [[CrossRef](#)]
26. Hsu, C.-H.; Lin, C.-Y.; Chen, J.-X. Wear and Corrosion Performance of Ti-6Al-4V Alloy Arc-Coated TiN/CrN Nano-Multilayer Film. *Metals* **2023**, *13*, 907. [[CrossRef](#)]
27. Wang, F.; Wu, J. Applications of hard coatings. In *Modern Ion Plating Technology: Fundamentals and Applications*; Elsevier: Amsterdam, The Netherlands, 2023; pp. 411–429.
28. Akhter, R.; Bendavid, A.; Munroe, P. Microstructure, mechanical properties and optical reflectance of TiNiN films deposited on silicon substrates using cathodic arc evaporation. *Thin Solid Film.* **2023**, *777*, 139896. [[CrossRef](#)]
29. Li, K.Q.; Chen, L.; Hu, C.; Zhang, J.; Du, J.W. Structure, mechanical and thermal properties of CrAlBSiN coatings prepared by cathodic arc evaporation. *Surf. Coat. Technol.* **2023**, *452*, 129094. [[CrossRef](#)]
30. Sysyn, M.; Nabochenko, O.; Kovalchuk, V.; Przybyłowicz, M.; Fischer, S. Investigation of interlocking effect of crushed stone ballast during dynamic loading. *Rep. Mech. Eng.* **2021**, *2*, 65–76. [[CrossRef](#)]
31. Korznikova, E.; Schafner, E.; Steiner, G.; Zehetbauer, M.J. Measurements of vacancy type defects in SPD deformed Ni. In Proceedings of the TMS Annual Meeting, San Antonio, TX, USA, 12–16 March 2006; pp. 97–102.
32. Moradi Marjaneh, A.; Saadatmand, D.; Evazzade, I.; Babicheva, R.I.; Soboleva, E.G.; Srikanth, N.; Zhou, K.; Korznikova, E.A.; Dmitriev, S.V. Mass transfer in the Frenkel-Kontorova chain initiated by molecule impact. *Phys. Rev. E* **2018**, *98*, 023003. [[CrossRef](#)]
33. Babicheva, R.I.; Evazzade, I.; Korznikova, E.A.; Shepelev, I.A.; Zhou, K.; Dmitriev, S.V. Low-energy channel for mass transfer in Pt crystal initiated by molecule impact. *Comput. Mater. Sci.* **2019**, *163*, 248–255. [[CrossRef](#)]
34. Korznikova, G.; Korznikova, E.; Nazarov, K.; Shayakhmetov, R.; Khisamov, R.; Khalikova, G.; Mulyukov, R. Structure and Mechanical Behavior of Al-Nb Hybrids Obtained by High-Pressure-Torsion-Induced Diffusion Bonding and Subsequent Annealing. *Adv. Eng. Mater.* **2021**, *23*, 2000757. [[CrossRef](#)]
35. Shlyakhova, G.V.; Bochkareva, A.V.; Nadezhkin, M.V. Effect of Heat Treatment on Microstructure and Mechanical Properties of the Precipitation Hardening Elinvar Alloy. *Russ. Phys. J.* **2021**, *64*, 838–843. [[CrossRef](#)]
36. Astafurova, E.G.; Astafurov, S.V.; Reunova, K.A.; Melnikov, E.V.; Moskvina, V.A.; Panchenko, M.Y.; Maier, G.G.; Rubtsov, V.E.; Kolubaev, E.A. Structure Formation in Vanadium-Alloyed Chromium-Manganese Steel with a High Concentration of Interstitial Atoms C + N = 1.9 wt % during Electron-Beam Additive Manufacturing. *Phys. Mesomech.* **2022**, *25*, 1–11. [[CrossRef](#)]
37. Mulyukov, K.Y.; Korznikova, G.F.; Sagdatkireyeva, M.B.; Timofeyev, V.N.; Valiev, R.Z. The study of domain structure of submicron grained cobalt and its changes during heating. *J. Magn. Magn. Mater.* **1992**, *110*, 73–79. [[CrossRef](#)]
38. Mulyukov, K.Y.; Korznikova, G.F.; Nikitin, S.A. Magnetization of nanocrystalline dysprosium: Annealing effects. *J. Appl. Phys.* **1996**, *79*, 8584–8587. [[CrossRef](#)]
39. Yang, X.; Liu, S.; Wei, X.; Pan, B. Effects of annealing on the structure and microhardness of nanocrystalline Ni-Mn electrodeposits. *J. Alloys Compd.* **2023**, *960*, 170732. [[CrossRef](#)]

Disclaimer/Publisher’s Note: The statements, opinions and data contained in all publications are solely those of the individual author(s) and contributor(s) and not of MDPI and/or the editor(s). MDPI and/or the editor(s) disclaim responsibility for any injury to people or property resulting from any ideas, methods, instructions or products referred to in the content.